Keyong Wang
School of Mechanical Engineering,
Shanghai University of Engineering Science,
Shanghai 201620, China

Kambiz Vafai[1]
Fellow ASME
Department of Mechanical Engineering,
University of California,
Riverside, CA 92521

Peichao Li
School of Mechanical Engineering,
Shanghai University of Engineering Science,
Shanghai 201620, China

Hao Cen
Office of Campus Construction,
Tianjin Foreign Studies University,
Tianjin 300204, China

Forced Convection in a Bidisperse Porous Medium Embedded in a Circular Pipe

Compared to the regular (monodisperse) porous medium (MDPM) with one porosity scale, the bidisperse porous medium (BDPM) has two porosity scales, which may enhance the heat transfer capability. This work investigates the forced convective heat transport through a circular pipe filled with a BDPM. The two-velocity two-temperature model is utilized to describe the flow and temperature fields for both the fracture phase (macropores) and the porous phase (the matrix with micropores). The bidispersion effect is taken into account by altering the permeability of the porous phase in the medium. Analytical solutions of the velocities and temperatures for both phases are derived under the constant wall heat flux boundary condition. The local Nusselt number and heat transfer performance (HTP) are also developed to investigate how the bidispersivity affects the thermal characteristics over a wide range of parameter space. [DOI: 10.1115/1.4036574]

Keywords: bidisperse porous medium, local thermal nonequilibrium, forced convective heat transfer, circular pipe, heat transfer performance

1 Introduction

Precise prediction of porous-based thermal systems' performance has attracted considerable attention during the past several decades. Forced convective Nusselt number becomes higher when passages are filled with a porous material [1]. There are two primary models, namely local thermal equilibrium (LTE) and local thermal nonequilibrium (LTNE), which are utilized for representing the heat transport through a porous medium. The LTE model holds when the temperature difference between the solid and fluid phases is negligible, while the LTNE counterpart can capture the effects of substantial temperature differences. Numerous studies have been carried out for passages filled with regular porous media which have the fluid and solid phases [2–8]. Herein, a regular porous medium is also called a monodisperse porous medium (MDPM) which has one porosity scale.

Alternatively, a bidisperse porous medium (BDPM), informally defined by Chen et al. [9,10], consists of clusters of large particles which are agglomerations of small particles. This porous structure leads to a substantially higher area to volume ratio and consequently exhibits interesting thermal behavior. Compared to the MDPM, a BDPM has two scales of porosity representing macropores between the clusters and micropores within them. As such, a BDPM is usually looked as a regular porous medium in which the solid phase is replaced by another porous medium [11]. In keeping with the literature, the macropores are denoted by the f-phase and the remainder of the structure is done by the p-phase. Within a BDPM, the fluid occupies all of the f-phase and a fraction of the p-phase.

The bidisperse porous medium has been applied to absorbents for enhancing absorption performance or heat pipes for augmenting heat transfer rate [12–15]. Nield and Kuznetsov [11] proposed a two-velocity two-temperature model for investigating forced convection in a plane bidisperse porous channel coupled with conduction in plane slabs. Several analytical and numerical investigations have been carried out to uncover the thermal behavior of BDPM. Nield and Kuznetsov [16] utilized the two-velocity two-temperature model to investigate the forced convection in a parallel-plate channel fully filled with a BDPM. Two cases of uniform temperature and uniform heat flux at channel walls were studied. Local thermal equilibrium was assumed within the p-phase (each cluster), while local thermal nonequilibrium was assumed between the f- and p-phases. Subsequently, Nield and Kuznetsov [17] dealt with the thermally developing forced convection in a parallel-plate channel filled by a saturated bidispersed porous medium, with walls held at constant temperature. Further, Nield and Kuznetsov [18,19] studied symmetric and asymmetric heating configurations for a parallel-plate channel partially filled with a BDPM. For the case of asymmetric heating, a singular behavior of the Nusselt number was found and explained. Narasimhan and Reddy [20] utilized the bidisperse porous medium approach to analyze the thermal management of heat generating electronics which are modeled as microporous blocks separated by macrogaps in a channel. It was reported that the geometry and distribution of such a BDPM channel can be suitably tuned through the bidispersion parameters to augment the heat transfer and reduce the pressure drop. Later, Narasimhan et al. [21] extended the BDPM approach to treat the thermal management of data centers densely packed with heat generating electronic equipments. Ajay et al. [22] numerically studied the forced convection cooling of an electronic chip with and without a porous medium. Their study revealed that the average surface temperature of the electronic chip was reduced by 4.21 K using the bidisperse porous medium heat sink instead of the conventional one.

One of the earliest contributions to natural convective heat transfer in a BDPM was conducted by Nield and Kuznetsov [23] who employed the classical Rayleigh–Bénard theory for analyzing the onset of natural convection in a horizontal BDPM layer uniformly heated from below. Straughan [24] elaborated the possibility of oscillatory convection by revisiting the problem of thermal convection in a bidisperse porous medium. Nield and Kuznetsov [25] extended the classical Chen–Minkowycz study of convection past a vertical plate embedded in a MDPM to the case of a BDPM. They focused on the leading edge region and obtained a solution involving four BDPM parameters, namely the geometrical parameter, the interphase momentum transfer parameter, the porosity-modified thermal diffusivity ratio, and the permeability ratio. Rees et al. [26] numerically studied the same problem in which the effect of adopting two-velocity two-temperature model on the thermal fields in the close vicinity of the origin is discussed. Revnic et al. [27] investigated the steady Darcy-free convection in a square cavity filled with a BDPM. It was found that

[1]Corresponding author.

Contributed by the Heat Transfer Division of ASME for publication in the Journal of Heat Transfer. Manuscript received January 17, 2017; final manuscript received March 8, 2017; published online June 1, 2017. Editor: Portonovo S. Ayyaswamy.

the most important parameters that influence the fluid flow and heat transfer are the interphase heat transfer parameter and the modified thermal conductivity ratio. Narasimhan and Reddy [28] conducted a numerical study on the steady natural convection inside a square BDPM enclosure made from uniformly spaced, disconnected square porous blocks that form the microporous medium. Varying the number of blocks, macropore volume fraction and internal Darcy number generate the bidispersion effect. A correlation was developed to capture the bidispersion effects on the convective heat transfer of the BDPM enclosure. Subsequently, Narasimhan and Reddy [29] numerically dealt with the natural convection resonance inside the square BDPM enclosure subject to the time-periodic heat flux at a side wall, with the opposite wall kept isothermal while the top and bottom walls are adiabatic. It was reported that as the bidispersivity decreases, the time to reach steady oscillatory state decreases and is the shortest at the monodisperse porous medium enclosure limit. Also, an increase in the bidispersion effect due to an increase in the external permeability brought in by increasing the external porosity (fraction of macropores) leads to a rise in the resonance frequency.

Porous inserts enhance the heat transfer rate at the expense of the pressure drop. Cekmer et al. [30] introduced a definition of HTP under LTE condition in order to find a compromise between the heat transfer enhancement and pressure drop cost. Mahmoudi et al. [31] analytically treated a partially filled porous parallel-plate channel utilizing two different porous–fluid interface models (models A and B) under LTNE condition. It was concluded that the fraction of 0.7 of porous insertion reaches an optimal HTP. Wang et al. [32] numerically studied the gradient porous materials. Most recently, Wang et al. [33] extended the HTP study to the case of slip flow regime based on models A and B. They confirmed that the gas rarefaction negatively impacts the heat transfer capacity and has little influence on the optimal porous thickness. Dehghan et al. [34] analytically investigated the HTP for microchannels filled with porous media in the slip flow regime. It was reported that the HTP for hyper-porous media are almost greater than unity. The conduction thermal resistance of the walls has negligible influence on the HTP.

From a heat transfer point of view, the bidispersion configuration can be more advantageous than the monodispersion one. In the open literature, most contributions to forced convection focus on the parallel-plate channels filled with Darcian BDPMs. To authors' best knowledge, there is lack of studies in forced convection in non-Darcian BDPM passages. Moreover, no analytical, numerical, or experimental investigations have been presented on the HTP of a BDPM passage. With these motivations in mind, the present study aims to examine the thermally fully developed forced convective heat transfer inside a circular pipe filled with a non-Darcian BDPM. The effects of pertinent parameters, such as the Biot number, the effective thermal conductivity ratio, the Darcy number, and the interphase momentum transfer coefficient on the heat transfer behavior, are discussed. An alternative HTP is defined to determine in what range of Biot number and effective thermal conductivity ratio the BDPM circular pipe performs better than the MDPM one.

2 Mathematical Modeling

2.1 Governing Equations and Boundary Conditions. The working fluid flows through a bidisperse porous medium embedded in a circular pipe as depicted in Fig. 1. The impermeable wall is uniformly heated by a constant heat flux q_w, which is positive when the fluid is heated, and negative when the fluid is cooled. The flow is induced by a constant pressure gradient in the direction of the flow. The following assumptions are invoked in the current study:

- The steady-state hydrodynamically and thermally fully developed conditions are considered with temperature-independent properties.

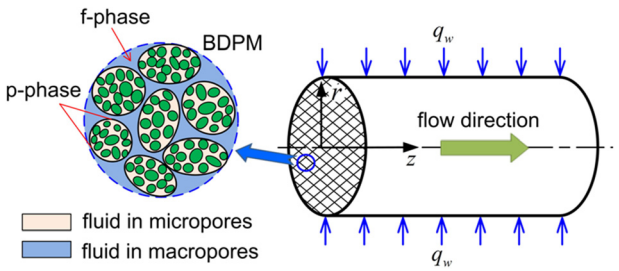

Fig. 1 Configuration of a circular pipe filled with a bidisperse porous medium

- Flows in the f- and p-phases of BDPM are both described by the Darcy-extended Brinkman momentum equations.
- Natural convection, dispersion, and radiative heat transfer are negligible.
- Axial conduction of the fluid within both phases is negligible when the Péclet number (Pe) is higher than unity, i.e., $O(\mathrm{Pe}) > 1$ [34].
- Local thermal equilibrium within the p-phase is valid while local thermal nonequilibrium between the f- and p-phases is allowed.

Bearing in mind the foregoing assumptions and considering the works of Magyari [35], Nield and Kuznetsov [16,36], and Cheng [37], the governing equations for the f- and p-phases of a BDPM thermal system are given by

Momentum equations:

$$\mu_{\mathrm{f,eff}}\frac{1}{r}\frac{\partial}{\partial r}\left(r\frac{\partial u_{\mathrm{f}}}{\partial r}\right)-\frac{\mu}{K_{\mathrm{f}}}u_{\mathrm{f}}+\zeta_{\mathrm{pf}}(u_{\mathrm{p}}-u_{\mathrm{f}})-\frac{\partial p}{\partial z}=0 \tag{1}$$

$$\mu_{\mathrm{p,eff}}\frac{1}{r}\frac{\partial}{\partial r}\left(r\frac{\partial u_{\mathrm{p}}}{\partial r}\right)-\frac{\mu}{K_{\mathrm{p}}}u_{\mathrm{p}}-\zeta_{\mathrm{pf}}(u_{\mathrm{p}}-u_{\mathrm{f}})-\frac{\partial p}{\partial z}=0 \tag{2}$$

Energy equations:

$$k_{\mathrm{f,eff}}\frac{1}{r}\frac{\partial}{\partial r}\left(r\frac{\partial T_{\mathrm{f}}}{\partial r}\right)+h_{\mathrm{pf}}(T_{\mathrm{p}}-T_{\mathrm{f}})=\rho c_{\mathrm{P}}u_{\mathrm{f}}\frac{\partial T_{\mathrm{f}}}{\partial z} \tag{3}$$

$$k_{\mathrm{p,eff}}\frac{1}{r}\frac{\partial}{\partial r}\left(r\frac{\partial T_{\mathrm{p}}}{\partial k}\right)-h_{\mathrm{pf}}(T_{\mathrm{p}}-T_{\mathrm{f}})=\rho c_{\mathrm{P}}u_{\mathrm{p}}\frac{\partial T_{\mathrm{p}}}{\partial z} \tag{4}$$

where u_{f} is the velocity in the f-phase physically representing the filtration velocity in the macropores, while u_{p} is the velocity in the p-phase denoting the effective velocity in the remainder of the structure, μ is the dynamic viscosity, K_{f} and K_{p} are the permeabilities in both phases; p is the applied pressure; ζ_{pf} is the interphase momentum transfer coefficient; T_{f}, T_{p}, ρ, and c_{p} are the f- and p-phase temperatures, density, and specific heat of the fluid, respectively; h_{pf} is the interphase heat transfer coefficient depending on the nature of the porous matrix and the saturating fluid; $k_{\mathrm{f,eff}}$ and $k_{\mathrm{p,eff}}$ are the effective thermal conductivities of both phases which can be classically determined by the following relation:

$$k_{\mathrm{f,eff}}=\varphi k_{\mathrm{f}},\quad k_{\mathrm{p,eff}}=(1-\varphi)k_{\mathrm{p}} \tag{5}$$

in which φ is the volume fraction of f-phase. It is noticeable that φ would be the porosity of the medium if the p-phase became solid [16]. In other words, a regular porous medium corresponds to the limiting case where the permeability of p-phase in a BDPM is sufficiently small.

The symmetry conditions at the centerline, $r = 0$, can be expressed as

$$\left.\frac{\partial u_f}{\partial r}\right|_{r=0} = \left.\frac{\partial u_p}{\partial r}\right|_{r=0} = 0 \tag{6}$$

$$\left.\frac{\partial T_f}{\partial r}\right|_{r=0} = \left.\frac{\partial T_p}{\partial r}\right|_{r=0} = 0 \tag{7}$$

At the pipe wall, $r = R$, the nonslip boundary conditions for the velocities can be expressed as

$$u_f|_{r=R} = u_p|_{r=R} = 0 \tag{8}$$

Based on the works of Amiri et al. [38] and Yang and Vafai [3], when a solid wall with finite thickness and high thermal conductivity is attached to a MDPM, the imposed heat flux q_w will be split between the fluid and solid phases depending on their effective conductivities and corresponding temperature gradients at the wall. Following a similar procedure, one can readily express the heat flux splitting between the f- and p-phases at the circular pipe wall–BDPM interface as

$$k_{f,eff}\left.\frac{\partial T_f}{\partial r}\right|_{r=R} + k_{p,eff}\left.\frac{\partial T_p}{\partial r}\right|_{r=R} = q_w \tag{9}$$

Meanwhile, the temperature of each phase at the wall is considered to be identical and equals to the wall temperature due to the low thermal resistance

$$T_f|_{r=R} = T_p|_{r=R} = T_w \tag{10}$$

where T_w denotes the wall temperature which is not known a priori and must be obtained as part of the solution.

2.2 Hydrodynamic Analysis. By introducing the following dimensionless variables

$$\eta = \frac{r}{R}, \quad U_f = \frac{\mu u_f}{GR^2}, \quad U_p = \frac{\mu u_p}{GR^2}, \quad G = -\frac{\partial p}{\partial z}, \quad M_f = \frac{\mu_{f,eff}}{\mu},$$
$$M_p = \frac{\mu_{p,eff}}{\mu}, \quad \psi = \frac{\zeta_{pf}R^2}{\mu}, \quad \mathrm{Da}_f = \frac{K_f}{R^2}, \quad \mathrm{Da}_p = \frac{K_p}{R^2} \tag{11}$$

the f- and p-phase momentum Eqs. (1) and (2) along with the boundary conditions given by Eqs. (6) and (8) can be rendered dimensionless as

$$M_f\frac{1}{\eta}\frac{\partial}{\partial\eta}\left(\eta\frac{\partial U_f}{\partial\eta}\right) - \frac{U_f}{\mathrm{Da}_f} + \psi(U_p - U_f) + 1 = 0 \tag{12}$$

$$M_p\frac{1}{\eta}\frac{\partial}{\partial\eta}\left(\eta\frac{\partial U_p}{\partial\eta}\right) - \frac{U_p}{\mathrm{Da}_p} - \psi(U_p - U_f) + 1 = 0 \tag{13}$$

$$\left.\frac{\partial U_f}{\partial\eta}\right|_{\eta=0} = \left.\frac{\partial U_p}{\partial\eta}\right|_{\eta=0} = 0 \tag{14}$$

$$U_f|_{\eta=1} = U_p|_{\eta=1} = 0 \tag{15}$$

With the notation

$$A_1 = \psi + \frac{1}{\mathrm{Da}_f}, \quad B_1 = \psi + \frac{1}{\mathrm{Da}_p} \tag{16}$$

and the formula

$$U_f(\eta) = A_2 + V(\eta) \tag{17}$$

$$U_p(\eta) = B_2 + W(\eta) \tag{18}$$

the two momentum Eqs. (12) and (13) can be converted to the matrix form

$$\begin{bmatrix} M_fL - A_1 & \psi \\ \psi & M_pL - B_1 \end{bmatrix}\begin{Bmatrix} V \\ W \end{Bmatrix} = 0 \tag{19}$$

where Da_f and Da_p are the Darcy numbers for the f- and p-phases in the bidisperse porous medium, respectively, L is the differential operator such that $L = (1/\eta)(\partial/\partial\eta)(\eta(\partial/\partial\eta))$ and

$$A_2 = \frac{(1+2\psi\mathrm{Da}_p)\mathrm{Da}_f}{1+\psi(\mathrm{Da}_f+\mathrm{Da}_p)}, \quad B_2 = \frac{(1+2\psi\mathrm{Da}_f)\mathrm{Da}_p}{1+\psi(\mathrm{Da}_f+\mathrm{Da}_p)} \tag{20}$$

The normal mode analysis proposed by Magyari [35] for the parallel-plate BDPM channel is adopted for the BDPM circular pipe in what follows. Constructing the eigenequation of coefficient matrix in Eq. (19) gives the independent eigenvector

$$\mathbf{S} = \begin{bmatrix} -\Omega & 1 \\ 1 & \Omega \end{bmatrix} \tag{21}$$

where

$$\Omega = \frac{(M_p - M_f)L + A_1 - B_1}{2\psi} + \sqrt{1 + \left[\frac{(M_p - M_f)L + A_1 - B_1}{2\psi}\right]^2} \tag{22}$$

Without loss of generality, a common practice assuming that $\mu_{f,eff} = \mu_{p,eff} = \mu$ and consequently $M_p = M_f = 1$ is utilized. As such, Eq. (22) can be simplified as

$$\Omega = \frac{A_1 - B_1}{2\psi} + \sqrt{1 + \left(\frac{A_1 - B_1}{2\psi}\right)^2} \tag{23}$$

The matrix-similarity transformation is performed on Eq. (19) to produce

$$\mathbf{S}^{-1}\begin{bmatrix} L - A_1 & \psi \\ \psi & L - B_1 \end{bmatrix}\mathbf{S}\begin{Bmatrix} Z_1 \\ Z_2 \end{Bmatrix} = 0 \tag{24}$$

where $\mathbf{S}^{-1}$ is the inverse of matrix $\mathbf{S}$ and

$$\begin{Bmatrix} Z_1 \\ Z_2 \end{Bmatrix} = \mathbf{S}^{-1}\begin{Bmatrix} V \\ W \end{Bmatrix} \tag{25}$$

After the above mathematical manipulations, Eq. (19) is diagonalized as

$$\begin{bmatrix} L - \omega_1^2 & 0 \\ 0 & L - \omega_2^2 \end{bmatrix}\begin{Bmatrix} Z_1 \\ Z_2 \end{Bmatrix} = 0 \tag{26}$$

where

$$\omega_{1,2}^2 = \psi\left[\frac{A_1 + B_1}{2\psi} \pm \sqrt{1 + \left(\frac{A_1 - B_1}{2\psi}\right)^2}\right] \tag{27}$$

and where $\omega_{1,2}$ denote the bidisperse porous medium shape factors for the p- and f-phases, respectively. To this end, the dimensionless momentum Eqs. (12) and (13) are decoupled for the normal modes Z_1 and Z_2 as

$$\frac{1}{\eta}\frac{\partial}{\partial\eta}\left(\eta\frac{\partial Z_{1,2}}{\partial\eta}\right) - \omega_{1,2}^2 Z_{1,2} = 0 \tag{28}$$

which admit the general solutions in terms of the zeroth order modified Bessel function of the first kind I_0

$$Z_{1,2} = C_{1,2}I_0(\omega_{1,2}\,\eta) \tag{29}$$

By substituting Eqs. (25) and (29) into Eqs. (17) and (18), we can analytically obtain the closed-form dimensionless velocity distributions for the f- and p-phases

$$U_{\mathrm{f}} = A_2 - \Omega Z_1 + Z_2 = A_2 - \Omega C_1 I_0(\omega_1 \eta) + C_2 I_0(\omega_2 \eta) \quad (30)$$

$$U_{\mathrm{p}} = B_2 + Z_1 + \Omega Z_2 = B_2 + C_1 I_0(\omega_1 \eta) + \Omega C_2 I_0(\omega_2 \eta) \quad (31)$$

Incorporating the dimensionless boundary conditions given by Eqs. (14) and (15) yields the integration constants C_1 and C_2

$$C_1 = \frac{A_2\,\Omega - B_2}{(1+\Omega^2) I_0(\omega_1)} \quad (32)$$

$$C_2 = -\frac{A_2 + B_2 \Omega}{(1+\Omega^2) I_0(\omega_2)} \quad (33)$$

2.3 Heat Transfer Analysis. The solution procedure is similar to the process utilized to solve a fluid saturated monodisperse porous medium under the LTNE condition. The coupled energy Eqs. (3) and (4) are added and then the resultant equation is integrated over the circular cross section of the pipe incorporating associated boundary conditions given by Eqs. (7) and (9) to yield

$$\frac{\partial T_{\mathrm{f}}}{\partial z} = \frac{\partial T_{\mathrm{p}}}{\partial z} = \frac{\partial T_{\mathrm{w}}}{\partial z} = \frac{\partial T_{\mathrm{b}}}{\partial z} = \frac{2 q_{\mathrm{w}}}{\rho c_{\mathrm{p}} R \langle u_+ \rangle} \quad (34)$$

where $\langle u_+ \rangle = (2/R^2) \int_0^R (u_{\mathrm{f}} + u_{\mathrm{p}})\, r dr$. It should be noted that the heat transfer occurs based on a velocity that is the cross-sectional average of the sum of f- and p-phase filtration velocities rather than the volume average of these velocities. This was also highlighted by Nield and Kuznetsov [16] who dealt with an isoflux parallel-plate channel filled with a BDPM. To facilitate the analytical solution for a broad number of thermophysical parameters, the following dimensionless variables are introduced as

$$\kappa = \frac{k_{\mathrm{f,eff}}}{k_{\mathrm{p,eff}}}, \quad \mathrm{Bi} = \frac{h_{\mathrm{pf}} R^2}{k_{\mathrm{p,eff}}}, \quad \hat{u}_{\mathrm{f}} = \frac{U_{\mathrm{f}}}{\langle U_+ \rangle}, \quad \hat{u}_{\mathrm{p}} = \frac{U_{\mathrm{p}}}{\langle U_+ \rangle}, \quad \theta = \frac{k_{\mathrm{p,eff}} (T - T_{\mathrm{w}})}{q_{\mathrm{w}} R} \quad (35)$$

By utilizing Eq. (34) and the variables defined in Eq. (35), it becomes possible to nondimensionize the energy Eqs. (3) and (4) along with the boundary conditions given by Eqs. (7) and (10) as

$$\kappa \frac{1}{\eta} \frac{\partial}{\partial \eta} \left(\eta \frac{\partial \theta_{\mathrm{f}}}{\partial \eta} \right) + \mathrm{Bi} (\theta_{\mathrm{p}} - \theta_{\mathrm{f}}) = 2 \hat{u}_{\mathrm{f}} \quad (36)$$

$$\frac{1}{\eta} \frac{\partial}{\partial \eta} \left(\eta \frac{\partial \theta_{\mathrm{p}}}{\partial \eta} \right) - \mathrm{Bi} (\theta_{\mathrm{p}} - \theta_{\mathrm{f}}) = 2 \hat{u}_{\mathrm{p}} \quad (37)$$

$$\left. \frac{\partial \theta_{\mathrm{f}}}{\partial \eta} \right|_{\eta=0} = \left. \frac{\partial \theta_{\mathrm{p}}}{\partial \eta} \right|_{\eta=0} = 0 \quad (38)$$

$$\theta_{\mathrm{f}}|_{\eta=1} = \theta_{\mathrm{p}}|_{\eta=1} = 0 \quad (39)$$

where κ is the effective thermal conductivity ratio, Bi is the Biot number representing strength of interphase heat transfer in a BDPM, and $\langle U_+ \rangle$ is the cross-sectional averaged value of the sum of f- and p-phase dimensionless velocities given by

$$\langle U_+ \rangle = 2 \int_0^1 (U_{\mathrm{f}} + U_{\mathrm{p}})\, \eta d\eta = A_2 + B_2 + \frac{2(1-\Omega) C_1}{\omega_1} I_1(\omega_1) + \frac{2(1+\Omega) C_2}{\omega_2} I_1(\omega_2) \quad (40)$$

The two dimensionless energy Eqs. (36) and (37) are solved subject to the boundary conditions given by Eqs. (38) and (39). Using the indirect decoupling procedure similar to the one for the MDPM parallel-plate channel [39], one can obtain the dimensionless temperature distributions for both phases in the radial direction as

$$\theta_{\mathrm{p}} = D_1 I_0(\omega_1 \eta) + D_2 I_0(\omega_2 \eta) + D_3 \eta^2 + D_4 - \kappa \theta_{\mathrm{f}} \quad (41)$$

$$\theta_{\mathrm{f}} = E_1 I_0(\lambda \eta) + E_2 I_0(\omega_1 \eta) + E_3 I_0(\omega_2 \eta) + E_4 \eta^2 + E_5 \quad (42)$$

where λ is shorthand for $\lambda = \sqrt{\mathrm{Bi}(1+\kappa)/\kappa}$, $D_1, \ldots, D_4$ and $E_1, \ldots, E_5$ are constants given by

$$D_1 = \frac{2(1-\Omega) C_1}{\omega_1^2 \langle U_+ \rangle} \quad (43)$$

$$D_2 = \frac{2(1+\Omega) C_2}{\omega_2^2 \langle U_+ \rangle} \quad (44)$$

$$D_3 = \frac{A_2 + B_2}{2 \langle U_+ \rangle} \quad (45)$$

$$D_4 = -[D_1 I_0(\omega_1) + D_2 I_0(\omega_2) + D_3] \quad (46)$$

$$E_1 = -\frac{1}{I_0(\lambda)} \left[E_2 I_0(\omega_1) + E_3 I_0(\omega_2) + E_4 + E_5 \right] \quad (47)$$

$$E_2 = \frac{\mathrm{Bi} D_1 \langle U_+ \rangle + 2\Omega C_1}{\kappa (\lambda^2 - \omega_1^2) \langle U_+ \rangle} \quad (48)$$

$$E_3 = \frac{\mathrm{Bi} D_2 \langle U_+ \rangle - 2 C_2}{\kappa (\lambda^2 - \omega_2^2) \langle U_+ \rangle} \quad (49)$$

$$E_4 = \frac{D_3}{1+\kappa} \quad (50)$$

$$E_5 = \frac{1}{1+\kappa} \left(\frac{4 D_3}{\lambda^2} + D_4 - \frac{2 A_2}{\mathrm{Bi} \langle U_+ \rangle} \right) \quad (51)$$

It is interesting to note that in the limit as $Da_{\mathrm{p}} \to 0$ (i.e., the p-phase becomes solid), Eqs. (41) and (42) will reduce to the non-slip regime solutions for monodisperse porous media obtained by Wang et al. [6].

2.4 Heat Transfer Performance. It is usual to capture the pressure-drop information in terms of the product of the friction factor f_r and the Reynolds number Re. Utilizing the velocities given by Eqs. (30) and (31), this product for the BDPM circular pipe can be expressed as

$$\mathrm{f}_r \mathrm{Re} = -\left(\mu \left. \frac{\partial \hat{u}}{\partial r} \right|_{r=R} \right) \Big/ \frac{1}{2} \left(\rho \langle U \rangle^2 \right) = 4 \left. \frac{\partial \hat{u}}{\partial \eta} \right|_{\eta=1} = \frac{4}{\langle U \rangle} \left\{ [\varphi \Omega - (1-\varphi)] C_1 \omega_1 I_1(\omega_1) - [\varphi + (1-\varphi)\Omega] C_2 \omega_2 I_1(\omega_2) \right\} \quad (52)$$

where $\langle U \rangle = 2 \int_0^1 [\varphi U_{\mathrm{f}} + (1-\varphi) U_{\mathrm{p}}]\, \eta d\eta$.

With the obtained solutions for θ_{f} and θ_{p}, the local Nusselt number which characterizes the heat transfer rate between the heated wall and the fluid can be evaluated. If the pipe radius is selected as the characteristic length, the convective heat transfer coefficient at the wall can be deduced from

$$\hbar = \frac{q_{\mathrm{w}}}{T_{\mathrm{w}} - T_{\mathrm{b}}} \quad (53)$$

As a result, based on the equivalent thermal conductivity of the BDPM, $k_{eq} = k_{f,eff} + k_{p,eff}$, the local Nusselt number Nu can be defined by

$$\mathrm{Nu} = -\frac{q_w(2R)}{k_{eq}(T_w - T_b)} = -\frac{2}{(1+\kappa)\theta_b} \tag{54}$$

where T_b and θ_b are the dimensional and dimensionless bulk mean fluid temperatures, respectively, which can be obtained by averaging over the circular cross section of the pipe as

$$T_b = \frac{2}{R^2\langle u\rangle}\int_0^R \left[\varphi u_f T_f + (1-\varphi)u_p T_p\right] r dr \tag{55}$$

$$\theta_b = 2\int_0^1 \left[\varphi \hat{u}_f \theta_f + (1-\varphi)\,\hat{u}_p \theta_p\right]\eta\, d\eta \tag{56}$$

in which $\langle u\rangle = (2/R^2)\int_0^R \left[\varphi u_f + (1-\varphi)u_p\right] r dr$.

Many studies have demonstrated that the heat transfer enhancement comes at the price of a pressure drop. To determine if the BDPM-filled circular pipe is better than the MDPM one, an alternative heat transfer performance is introduced as

$$\mathrm{HTP} = \frac{\mathrm{Nu}}{\mathrm{Nu}^*} \Big/ \frac{(f_r\mathrm{Re})}{(f_r\mathrm{Re})^*} = \frac{(f_r\mathrm{Re})^*\mathrm{Nu}}{(f_r\mathrm{Re})\mathrm{Nu}^*} \tag{57}$$

where the asterisk denotes the MDPM pipe parameters which are given in the Appendix.

3 Results and Discussion

3.1 Validation. For validating the present analytical solutions, we evaluate the dimensionless temperature correlation along the radial direction. In all of the following calculations, the volume fraction of f-phase is selected as $\varphi = 0.9$. When the permeability K_p of the p-phase approaches a very small value, i.e., $\mathrm{Da}_p \to 0$, and the interphase momentum transfer vanishes ($\psi \to 0$), the flow in the BDPM circular pipe would reduce to that in the MDPM one. For this limiting case ($\mathrm{Da}_p = \psi = 10^{-5}$), a comparison of the dimensionless temperature distributions ($\mathrm{Bi} = 0.5$, $\kappa = 0.1$) is performed with those derived by Dukhan et al. [40]. It is clearly seen from Fig. 2 that an excellent agreement is found between these results.

When the Biot number approaches infinity for a MDPM, the temperature difference between the solid and fluid phases would vanish due to the high effective interstitial heat transfer rate. To evaluate the Nusselt number under the local thermal equilibrium condition, one can add Eqs. (36) and (37) with $\theta_f = \theta_p = \theta_{LTE}$. In doing so, the LTE model for a BDPM circular pipe is obtained as

$$\frac{1}{\eta}\frac{\partial}{\partial\eta}\left(\eta\frac{\partial\theta_{LTE}}{\partial\eta}\right) = \frac{2}{1+\kappa}(\hat{u}_f + \hat{u}_p) \tag{58}$$

$$\left.\frac{\partial\theta_{LTE}}{\partial\eta}\right|_{\eta=0} = 0 \tag{59}$$

$$\theta_{LTE}|_{\eta=1} = 0 \tag{60}$$

Integrating Eq. (58) analytically twice, and then employing Eqs. (59) and (60), the LTE dimensionless temperature distribution is obtained as

$$\theta_{LTE} = \frac{2}{(1+\kappa)\langle U_+\rangle}\left\{\frac{(\Omega-1)C_1}{\omega_1^2}\left[I_0(\omega_1\eta) - I_0(\omega_1)\right] + \frac{(\Omega+1)C_2}{\omega_2^2}\left[I_0(\omega_2\eta) - I_0(\omega_2)\right] + \frac{1}{4}(A_2+B_2)(\eta^2-1)\right\} \tag{61}$$

For another verification, the fully developed Nusselt numbers for $\mathrm{Da}_f = 1$, $\mathrm{Da}_p \to 0$, and $\psi \to 0$ are compared with those calculated by Wang et al. [6]. These results are tabulated in Table 1. As can be seen, a very good agreement exists between the two results. It is apparent that the values of the BDPM Nusselt number are consistent with those of the MDPM one when the p-phase Darcy number and the interphase momentum transfer coefficient are sufficiently small.

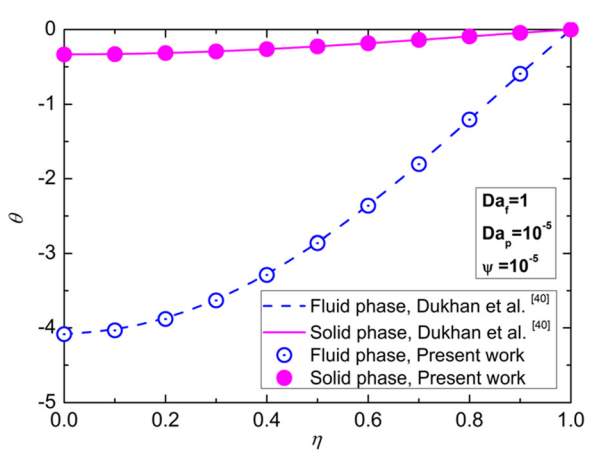

Fig. 2 Comparison of the present analytical dimensionless temperature distributions with those obtained by Dukhan et al. [40]

3.2 Temperature Distribution and Nusselt Number. Figure 3 compares the temperature distribution for different combinations of the Biot number and the effective thermal conductivity ratio using $(\mathrm{Da}_f, \mathrm{Da}_P) = (10^{-2}, 10^{-3})$. A monotonic increase in the dimensionless temperatures from the centerline to the heated wall is observed for both BDPM and MDPM pipes. From the MDPM limit ($\mathrm{Da}_p \to 0$), as Da_p increases, the maximum temperature difference between the f- and p-phases decreases. This is attributed to the fact that an increase in Da_p leads to the fluid permeating both the micro- and macropores. Once Da_p is greater than zero, the effect of bidispersion appears and hence the convection heat transfer is enhanced. On the other hand, by comparing Figs. 3(*a*) and 3(*b*), it is observed that increasing Biot number narrows the maximum temperature difference inside the porous medium due to the enhanced heat exchange between the f- and p-phases. This trend can also be confirmed by comparing Figs. 3(*c*) and 3(*d*). It is also concluded from all the subfigures that the maximum temperature difference within the porous medium decreases by increasing the value of κ from 0.1 to 10. This can be seen by comparing Figs. 3(*a*) and 3(*c*) as well as Figs. 3(*b*) and 3(*d*). For a given volume fraction of BDPM, i.e., $\varphi = 0.9$, an increase in κ means a rise in the fluid thermal conductivity. As it is seen in Fig. 3, by increasing κ, it may be possible to change the relationship between the temperatures of the f- and p-phases in magnitude. This phenomenon can be observed by comparing the temperature distributions for $\kappa = 0.1$ and 10, i.e., $T_f < T_p$ for $\kappa = 0.1$ whereas

Table 1 Comparison of the present analytical Nusselt numbers with those obtained by Wang et al. [6] for $(\mathrm{Da}_f, \mathrm{Da}_p) = (1, 10^{-5})$ and $\psi = 10^{-5}$

κ	Bi	Present work	Wang et al. [6]
0.01	0.01	0.05125	0.05125
0.01	1	0.68485	0.68478
100	0.01	4.37196	4.37151
100	1	4.37827	4.37787

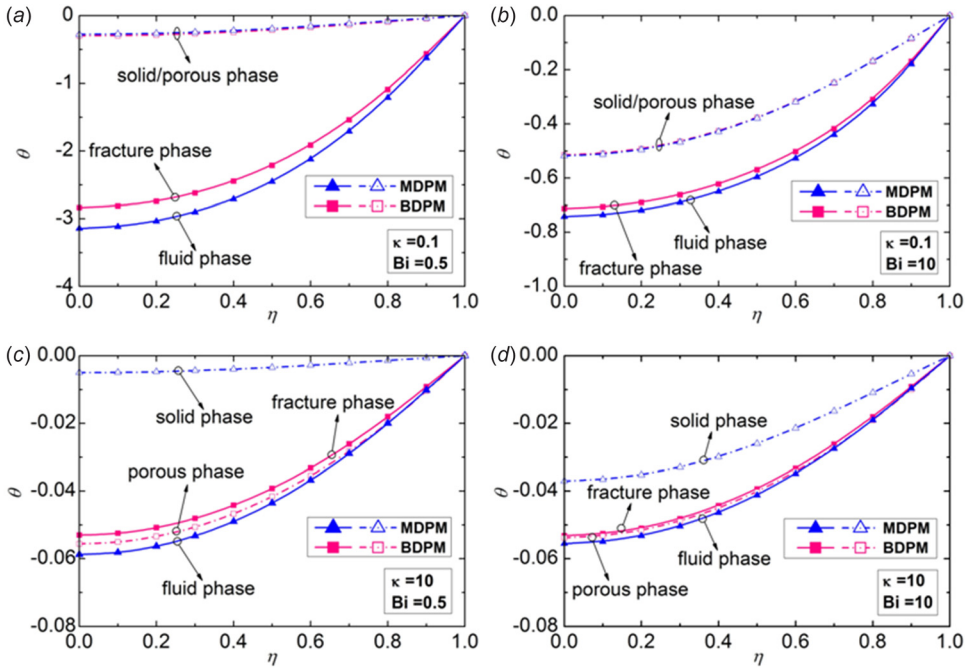

Fig. 3 Dimensionless temperature distributions at $(Da_f, Da_P) = (10^{-2}, 10^{-3})$ and $\psi = 1$: (*a*) $\kappa = 0.1$, Bi = 0.5; (*b*) $\kappa = 0.1$, Bi = 10; (*c*) $\kappa = 10$, Bi = 0.5; and (*d*) $\kappa = 10$, Bi = 10

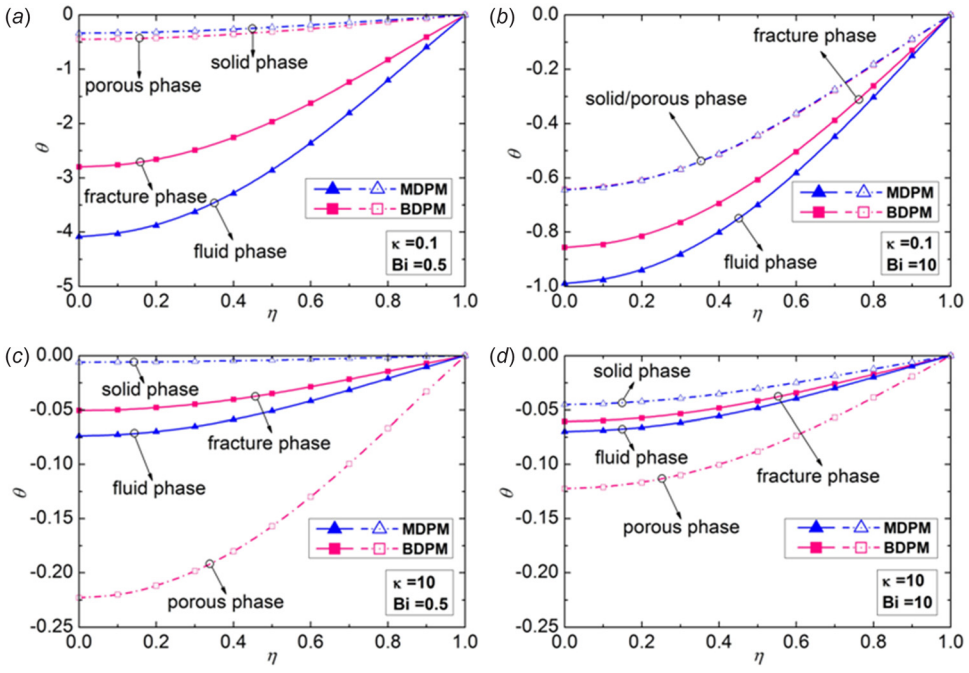

Fig. 4 Dimensionless temperature distributions at $(Da_f, Da_P) = (1, 0.1)$ and $\psi = 1$: (*a*) $\kappa = 0.1$, Bi = 0.5; (*b*) $\kappa = 0.1$, Bi = 10; (*c*) $\kappa = 10$, Bi = 0.5; and (*d*) $\kappa = 10$, Bi = 10

$T_f > T_p$ for $\kappa = 10$. It reveals that the effect of bidispersivity becomes more significant in heat transfer when changing κ from 0.1 to 10. For a monodisperse porous medium, however, the temperature of the solid phase would obey that of the fluid phase closer by increasing the effective thermal conductivity ratio κ. And the temperatures of both phases in a MDPM are expected to be identical when $\kappa \to \infty$. In a bidisperse porous medium, however, the temperatures are different. There exists a critical value of effective thermal conductivity ratio, κ_{cr}, which makes the f- and p-phase temperatures to be the same. When $\kappa < \kappa_{cr}$, as κ increases, the maximum temperature difference between the two phases decreases with $T_f < T_p$ whereas the trend is reversed when $\kappa > \kappa_{cr}$.

Figure 4 depicts the same type of information as Fig. 3 for extremely high Darcy numbers $(Da_f, Da_p) = (1, 0.1)$. For all of the combinations of Bi and κ, the temperature distribution exhibits a similar trend with that shown in Fig. 3 for lower Darcy numbers $(Da_f, Da_P) = (10^{-2}, 10^{-3})$. By comparing Figs. 3(*c*) and 4(*c*) as well as Figs. 3(*d*) and 4(*d*), it is seen that under the same parameter space the larger the Darcy numbers for the f- and p-phases in a

Table 2 Variation of κ_{cr} with the effect of bidispersivity at *Bi*=0.5

			κ_{cr}		
Da_f	Da_p	Υ	$\psi = 1$	$\psi = 10^2$	$\psi = 10^4$
0.01	2×10^{-3}	0.2	4.77162	2.31598	1.01990
	4×10^{-3}	0.4	2.41410	1.49348	1.00746
	6×10^{-3}	0.6	1.62839	1.21932	1.00332
	8×10^{-3}	0.8	1.23562	1.08226	1.00126
1	0.2	0.2	1.45330	1.01934	1.00021
	0.4	0.4	1.17009	1.00725	1.00009
	0.6	0.6	1.08072	1.00322	1.00005
	0.8	0.8	1.02835	1.00122	1.00002

BDPM, the temperature of the f-phase would be much higher than that of the p-phase except at the heated wall where the local thermal equilibrium holds. Table 2 illustrates the critical values of effective thermal conductivity ratio (κ_{cr}) for different combinations of Da_f and Da_p. Here, κ_{cr} is evaluated by equating the maximum temperature difference between the f- and p-phases to zero at the centerline, i.e., $[\theta_f(\kappa_{cr}) - \theta_p(\kappa_{cr})]|_{\eta=0} = 0$ and solving for the numerical values of κ_{cr}. For convenience, a simple parameter, $\Upsilon = \psi Da_p/Da_f$, is introduced to take into account the bidispersion intensity. It is apparent that as the bidispersion intensity increases, κ_{cr} decreases. Higher Υ leads to a larger contact area to volume ratio and a more significant momentum transfer between the fluid and the porous matrix in a BDPM. As a consequence, the heat in the f- and p-phases can be exchanged efficiently due to more fluid flushing into the micropores in the p-phase. Moreover, in the case of the same bidispersion intensity, a BDPM with higher permeability (or Darcy numbers) has a lower value of κ_{cr}. It is also found that when the interphase momentum transfer coefficient reaches as high as $\psi = 10^4$, the critical conductivity ratio leads approximately to $\kappa_{cr} = 1.0$ at $\varphi = 0.9$ whether the permeabilities in the two phases are high or low.

Figure 5 depicts the variations of the Nusselt number with the Biot number using Darcy numbers $(Da_f, Da_P) = (10^{-2}, 10^{-3})$. As seen in Fig. 5, at $Da_f = 10^{-2}$ and a given Biot number, the Nusselt number increases with an increase in the bidispersion intensity. It is seen from Fig. 5 that as the Biot number rises up to 100, the distributions of Nusselt number for both BDPM and MDPM pipes approach their asymptotic values, respectively, i.e., the LTE solutions. By comparing Figs. 5(*a*) and 5(*c*) as well as Figs. 5(*b*) and 5(*d*), it is apparent that when the bidispersion intensity becomes considerable, the Nusselt number is augmented. This is attributed to the strong interaction of the same fluid in micro- and macropores, resulting in more uniform localized distribution of velocities and consequently that of temperatures. For very high values of Bi, as expected, both BDPM and MDPM pipes can predict the LTE solutions. Under same circumstances, the heat transfer rate of BDPM pipe is higher than that of MDPM one due to the effect of bidispersivity.

Figure 6 shows the same type of information as Fig. 5 for very high Darcy numbers $(Da_f, Da_P) = (1, 0.1)$. Compared to the results shown in Fig. 5, increasing Da_f and Da_p simultaneously leads to a reduction in the Nusselt number. But the asymptotic characteristics varying with Bi are similar to the observations seen in Fig. 5. Another interesting conclusion can be obtained by looking through Figs. 6(*a*)–6(*d*). It is seen from Fig. 6(*a*) that the values of Nusselt number obtained for $Da_p = 0.01$ are lower than those obtained for $Da_p = 0.1$ when $Bi < 100$, while the situation is reversed when $Bi > 100$. Comparing Figs. 6(*b*), 6(*c*), 6(*d*) with 5(*b*), 5(*c*), 5(*d*) under the same bidispersion intensity, the higher the f-phase permeability, the more prominent will be the heat transfer rate decrease with an increase in the p-phase permeability. Once again, when Bi becomes very large, the Nusselt numbers for both BDPM and MDPM pipes approach asymptotically their LTE solutions.

Figure 7 depicts the variation of the Nusselt number with the effective thermal conductivity ratio using Darcy numbers $(Da_f, Da_P) = (10^{-2}, 10^{-3})$. As shown in Fig. 7, the Nusselt number variations belonging to the BDPM and MDPM pipes demonstrate distinguishable feature when the value of κ is greater than the critical effective thermal conductivity ratio mentioned before. For the BDPM configuration at $Da_P = 10^{-3}$ and 10^{-4}, as κ increases, Nu initially increases and then goes through peak values before steadily declining to zero. Beyond κ_{cr}, further increase

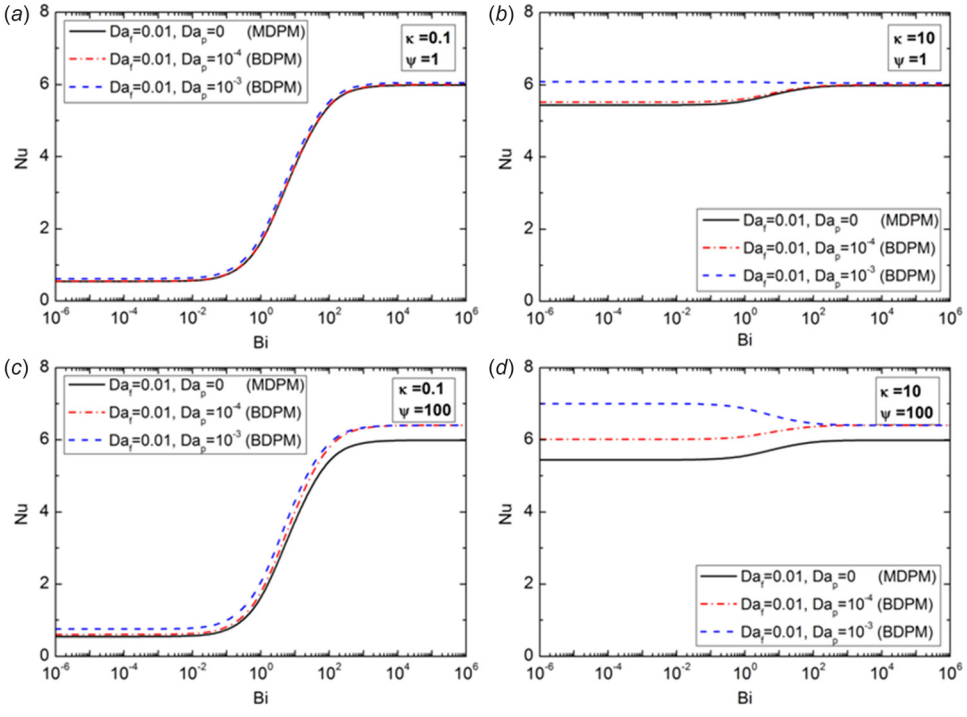

Fig. 5 Variation of the Nusselt number with the Biot number for different Darcy numbers: (*a*) $\kappa = 0.1$, $\psi = 1$; (*b*) $\kappa = 10$, $\psi = 1$; (*c*) $\kappa = 0.1$, $\psi = 100$; and (*d*) $\kappa = 10$, $\psi = 100$

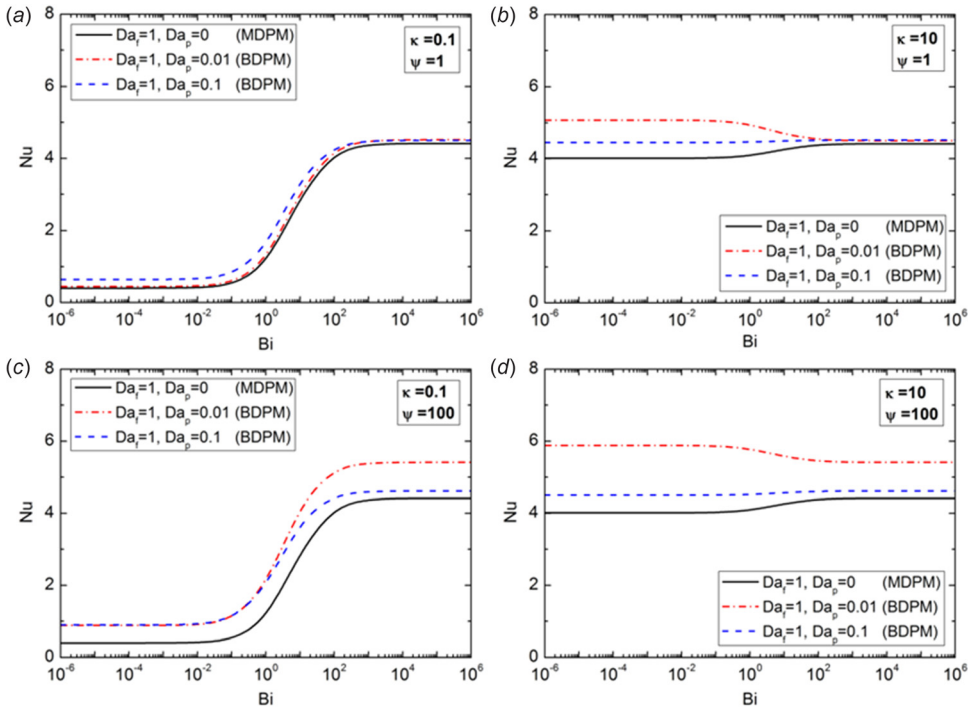

Fig. 6 Variation of the Nusselt number with the Biot number for very high Darcy numbers: (*a*) $\kappa = 0.1$, $\psi = 1$; (*b*) $\kappa = 10$, $\psi = 1$; (*c*) $\kappa = 0.1$, $\psi = 100$; and (*d*) $\kappa = 10$, $\psi = 100$

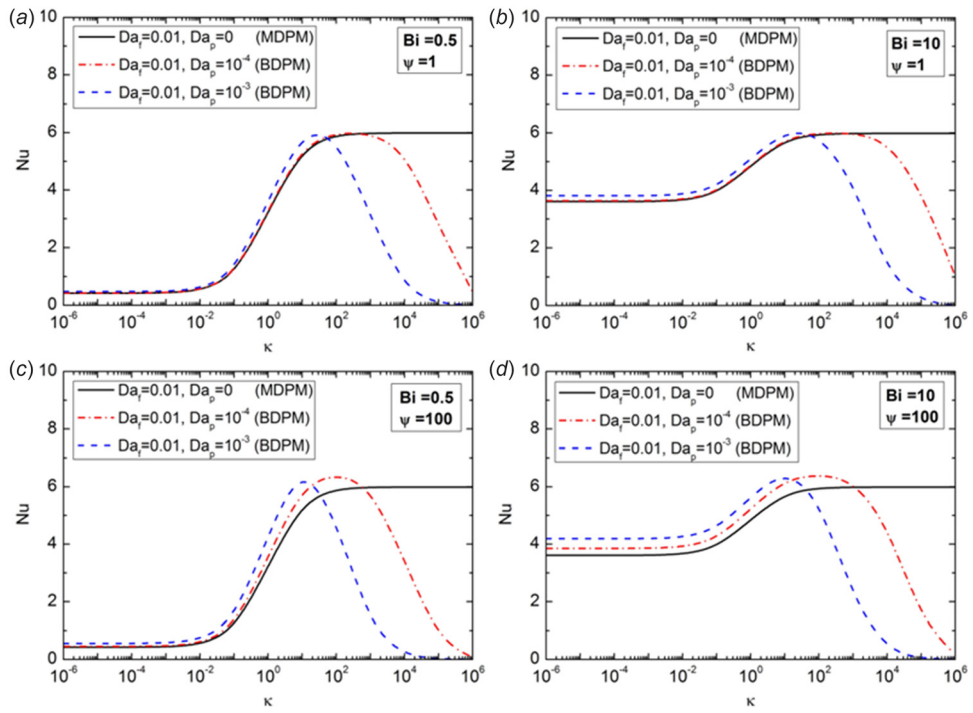

Fig. 7 Variation of the Nusselt number with the effective thermal conductivity ratio for different Darcy numbers: (*a*) Bi = 0.5, $\psi = 1$; (*b*) Bi = 10, $\psi = 1$; (*c*) Bi = 0.5, $\psi = 100$; and (*d*) Bi = 10, $\psi = 100$

in κ leads to the f-phase temperature being higher than the p-phase temperature and consequently a rapid reduction in the fluid bulk mean temperature. Hence, the Nusselt number decreases. A similar phenomenon was also reported by Nield and Kuznetsov [16] for a BDPM parallel-plate channel using Darcy's flow model. Another feature drawn from Fig. 7 is that the values of κ_{cr} are shifted toward the negative direction of the κ coordinate as the bidispersion intensity increases. More importantly, it is found that the results for a BDPM pipe are quite different from those for a MDPM one ($Da_p \rightarrow 0$). For the MDPM case, the cited threshold for κ does not exist. Unlike the BDPM, after passing the inclining stage, the MDPM distribution for Nu levels off upon further

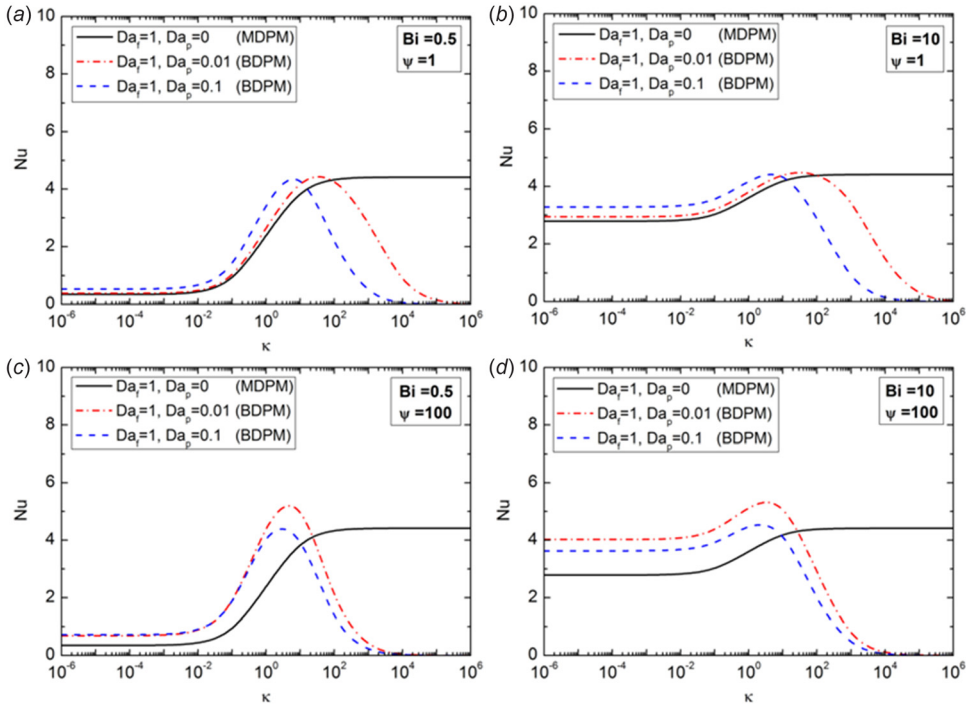

Fig. 8 Variation of the Nusselt number with the effective thermal conductivity ratio for very high Darcy numbers: (*a*) Bi = 0.5, $\psi = 1$; (*b*) Bi = 10, $\psi = 1$; (*c*) Bi = 0.5, $\psi = 100$; and (*d*) Bi = 10, $\psi = 100$

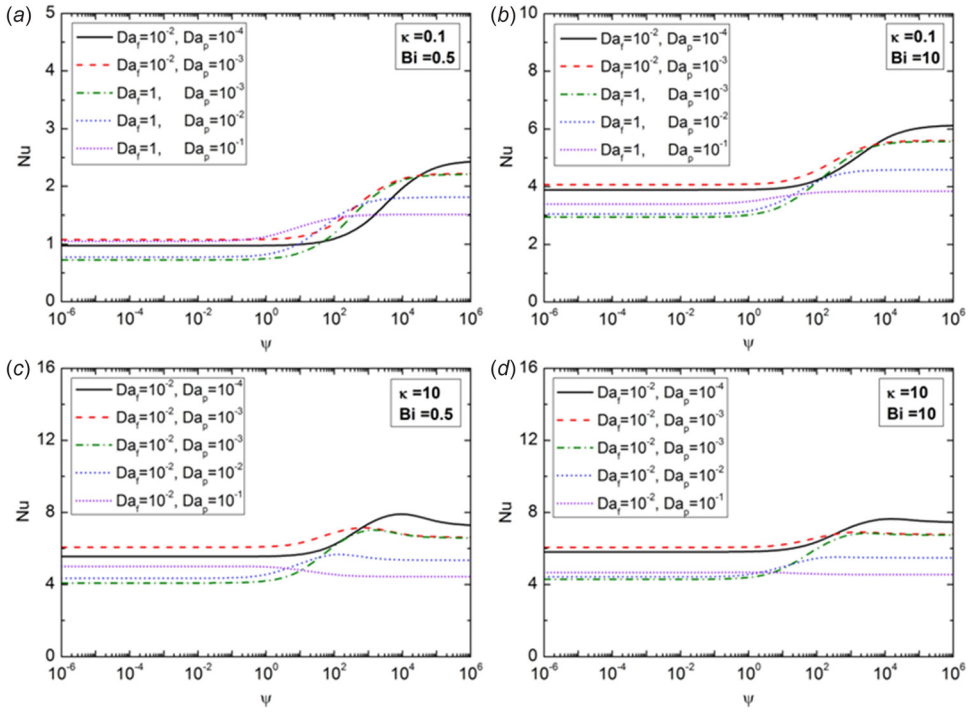

Fig. 9 Variation of the Nusselt number with the dimensionless momentum transfer coefficient for different combinations of Darcy numbers: (*a*) $\kappa = 0.1$, Bi = 0.5; (*b*) $\kappa = 0.1$, Bi = 10; (*c*) $\kappa = 10$, Bi = 0.5; and (*d*) $\kappa = 10$, Bi = 10

increase in κ due to the rapid heat transfer between the solid and fluid phases. As the effect of bidispersivity becomes marginal, say $Da_p > 0$, the fluid also flows into the micropores and redistributes the velocity field inside the BDPM and consequently the temperature fields in the f- and p-phases. For lower values of κ, as the effect of bidispersivity increases, the Nusselt number enhances whereas for higher values of κ, the trend is reversed.

Figure 8 shows the same type of information as in Fig. 7 for very high Darcy numbers $(Da_f, Da_P) = (1, 0.1)$. Compared to the results shown in Fig. 7, the increase in Da_f and Da_p

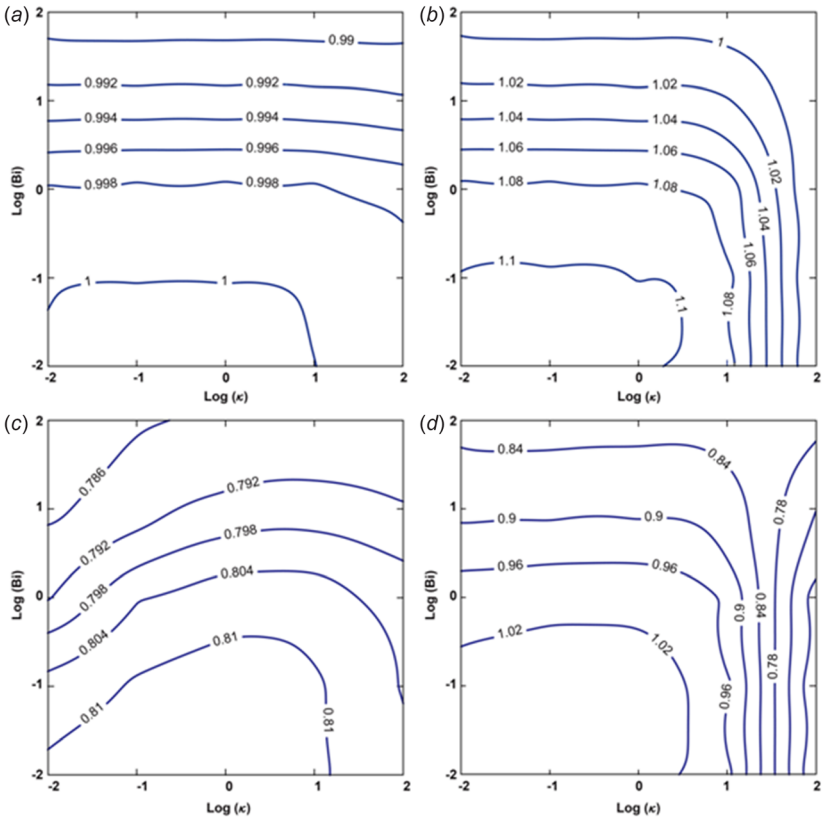

Fig. 10 Effect of Darcy numbers on the contours of HTP: (*a*) $\psi = 1$, $(Da_f, Da_p) = (10^{-2}, 10^{-4})$; (*b*) $\psi = 1$, $(Da_f, Da_P) = (10^{-2}, 10^{-3})$; (*c*) $\psi = 100$, $(Da_f, Da_p) = (10^{-2}, 10^{-4})$; and (*d*) $\psi = 100$, $(Da_f, Da_P) = (10^{-2}, 10^{-3})$

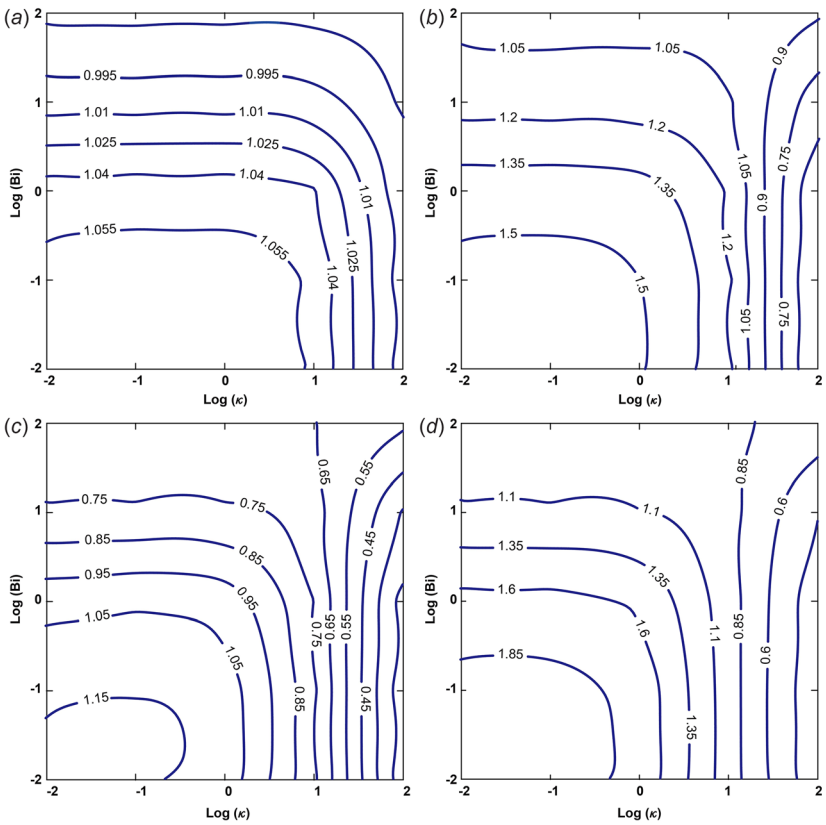

Fig. 11 Effect of very high Darcy numbers on the contours of HTP: (*a*) $\psi = 1$, $(Da_f, Da_p) = (1, 0.01)$; (*b*) $\psi = 1$, $(Da_f, Da_P) = (1, 0.1)$; (*c*) $\psi = 100$, $(Da_f, Da_p) = (1, 0.01)$; and (*d*) $\psi = 100$, $(Da_f, Da_P) = (1, 0.1)$

simultaneously leads to lower peak values of Nu for a BDPM pipe. It is seen from Figs. 8(*c*) and 8(*d*) that at lower values of κ, Nu decreases when the bidispersivity is enhanced. This reveals that for a high-permeability BDPM, the Nu trend can be reversed when there is substantial momentum transfer coupling between the f- and p-phases. For the MDPM pipe, the tendency is almost similar to that shown in Fig. 7 for lower Darcy numbers but the magnitude of Nu becomes smaller.

Figure 9 delineates the effect of interphase momentum transfer on the Nusselt number for different combinations of Da_f and Da_p. In the case of weak momentum transfer coupling between the two phases ($\psi = 10^{-6}$), the velocity distributions in the f- and p-phases in the BDPM would decay into almost two independent ones like a monodisperse porous medium. On the other hand, in the case of very strong coupling ($\psi = 10^{6}$), the velocity distributions approach each other. For a given Da_f with lower ψ, an increase in Da_p leads to an enhancement in Nu. But at higher values of ψ, an increase in Da_p results in a reduction in Nu. It is worth mentioning that the change in Nu is more marked when the value of ψ falls between 10 and 10^4. As is seen in all the subfigures, there exists an intersection point for any two values of Da_p based on the same value of Da_f, at which the same Nusselt number is obtained. It is noteworthy that this intersection point would take different values, which can be seen from the results for $(Da_f, Da_P) = (1, 10^{-3})$, $(1, 10^{-2})$ and $(1, 0.1)$ in Fig. 9. This explains the opposite features shown in Figs. 6 and 8. Moreover, a decrease in the interphase momentum transfer coefficient reduces the Nusselt number. In other words, the thermal nonequilibrium effects are strong for lower values of ψ.

3.3 Maps of the Heat Transfer Performance. With respect to the heat transfer performance, the maps of HTP for both lower and higher Darcy numbers are shown in Figs. 10 and 11. As shown in Fig. 10, when the values of Bi and κ are both small, the HTP would approach its maximum. Nevertheless, it is apparent that the heat transfer performance of a BDPM circular pipe does not exhibit a noticeable advantage over that of a MDPM one. For the case of very high Darcy numbers as depicted in Fig. 11, the HTP shows a similar trend as the case of lower Darcy numbers. It is noted that the values of HTP are enhanced under the same considered parameters. This implies that a BDPM pipe can obtain higher heat transfer rate compared to a MDPM one under certain circumstances.

4 Conclusions

Thermally developed forced convective heat transfer of a circular pipe filled with a bidisperse porous medium has been theoretically investigated utilizing the two-velocity two-temperature model. The analytical solutions for the velocity and temperature distributions in the f- and p-phases have been derived. It is found that the temperature distribution alters remarkably with the bidispersion intensity. The increasing effective thermal conductivity ratio signifies the maximum temperature difference between the two phases inside the medium. A critical value of the effective thermal conductivity ratio is observed, below which the temperature in the p-phase is higher than that in the f-phase whereas beyond which the situation is reversed due to the bidispersivity. At κ_{cr}, the temperature difference between the two phases vanishes because the local thermal equilibrium governs the thermal system. A comprehensive discussion regarding the effects of pertinent thermophysical parameters on the Nusselt number is also presented. Before approaching the critical conductivity ratio, the Nusselt number increases with an increase in the effective thermal conductivity ratio. But after passing the critical point, the BDPM Nusselt number drops sharply down to zero. On the contrary, the MDPM pipe generally exhibits the asymptotic behavior when the effective thermal conductivity ratio becomes large. In addition, the BDPM pipe with very high Darcy numbers gives rise to higher HTP than the MDPM one. However, in general for regular Darcy numbers, BDPM does not display an advantage over the MDPM one.

Acknowledgment

This work was supported by the Construction Program of Local Colleges and Universities from Science and Technology Commission of Shanghai (Grant No. 14110501200). The authors would like to acknowledge this support.

Nomenclature

- Bi = Biot number, $h_{pf}R^2/k_{p,eff}$
- c_P = specific heat of the fluid (J kg^{-1} K^{-1})
- Da = Darcy number
- f_r = friction factor
- h_{pf} = interphase heat transfer coefficient (W m^{-3} K^{-1})
- K = permeability (m^2)
- k_f = thermal conductivity of the f-phase (W m^{-1} K^{-1})
- $k_{f,eff}$ = effective thermal conductivity of the f-phase (W m^{-1} K^{-1})
- k_p = thermal conductivity of the p-phase (W m^{-1} K^{-1})
- $k_{p,eff}$ = effective thermal conductivity of the p-phase (W m^{-1} K^{-1})
- M = ratio of the effective to actual viscosity of the fluid, μ_{eff}/μ
- Nu = local Nusselt number at the pipe wall
- p = pressure (Pa)
- q_w = imposed heat flux on the pipe wall (W m^{-2})
- r = radial coordinate
- R = radius of the circular pipe (m)
- Re = Reynolds number
- T = temperature (K)
- u = velocity of the fluid (m s^{-1})
- U = dimensionless velocity of the fluid
- z = axial coordinate

Greek Symbols

- η = dimensionless radial coordinate, r/R
- θ = dimensionless temperature, $k_{p,eff}(T - T_w)/q_wR$
- κ = ratio of the effective thermal conductivity of the f-phase to that of the p-phase, $k_{f,eff}/k_{p,eff}$
- λ = $\sqrt{\mathrm{Bi}(1+\kappa)/\kappa}$
- μ = dynamic viscosity (Pa·s)
- ρ = density of the fluid (kg m^{-3})
- φ = volume fraction of the f-phase

Subscripts

- eff = effective
- f = f-phase
- p = p-phase
- w = pipe wall subject to a constant heat flux
- $\langle\ \rangle$ = average of a quantity

Appendix

The dimensionless velocity distribution in a MDPM circular pipe subject to the no-slip condition is given by

$$\hat{u}^* = \frac{\omega\left[I_0(\omega) - I_0(\omega\eta)\right]}{\omega I_0(\omega) - 2I_1(\omega)} \tag{A1}$$

where ω is the monodisperse porous medium shape factor. Following a similar procedure introduced in Eq. (52) for the BDPM pipe, we can find the pressure drop cost for the MDPM one

$$(f_r\mathrm{Re})^* = 4\left|\frac{\partial\hat{u}^*}{\partial\eta}\right|_{\eta=1} = \frac{4\omega^2 I_1(\omega)}{\omega I_0(\omega) - 2I_1(\omega)} \tag{A2}$$

Considering the continuum flow (no-slip flow) regime addressed by Wang et al. [6] and after some mathematical manipulations, the local Nusselt number for a MDPM circular pipe under LTNE condition can be presented as

$$\mathrm{Nu}^* = \frac{2}{(1+\kappa)F_5}\left\{\begin{array}{l}\left\{\dfrac{1}{\lambda^2-\omega^2}\left[\lambda I_1(\lambda)I_0(\omega)-\omega I_0(\lambda)I_1(\omega)\right]-\dfrac{I_1(\lambda)I_0(\omega)}{\lambda}\right\}F_1\\ +\left\{\dfrac{1}{2}\left[I_0^2(\omega)-I_1^2(\omega)\right]-\dfrac{I_0(\omega)I_1(\omega)}{\omega}\right\}F_2+\left[\dfrac{2I_2(\omega)}{\omega^2}+\dfrac{I_3(\omega)}{\omega}-\dfrac{I_0(\omega)}{4}\right]F_3\\ +\left[\dfrac{I_1(\omega)}{\omega}-\dfrac{I_0(\omega)}{2}\right]F_4\end{array}\right\}^{-1} \tag{A3}$$

where I_1, I_2, and I_3 are the first-, second-, and third-order modified Bessel functions of the first kind, respectively, and F_1,..., F_5 are constants given by

$$F_1 = -\frac{F_2 I_0(\omega)+F_3+F_4}{I_0(\lambda)} \tag{A4}$$

$$F_2 = \frac{F_5}{\kappa(\lambda^2-\omega^2)}\left(1-\frac{\mathrm{Bi}}{\omega^2}\right) \tag{A5}$$

$$F_3 = \frac{F_5}{4(1+\kappa)}I_0(\omega) \tag{A6}$$

$$F_4 = \frac{F_5}{1+\kappa}\left(\frac{1}{\lambda^2}+\frac{1}{\omega^2}-\frac{1}{\mathrm{Bi}}-\frac{1}{4}\right)I_0(\omega) \tag{A7}$$

$$F_5 = \frac{2\omega}{\omega I_0(\omega)-2I_1(\omega)} \tag{A8}$$

References

[1] Satyamurty, V. V., and Bhargavi, D., 2010, "Forced Convection in Thermally Developing Region of a Channel Partially Filled With a Porous Material and Optimal Porous Fraction," Int. J. Therm. Sci., **49**(2), pp. 319–332.

[2] Nield, D. A., Kuznetsov, A. V., and Xiong, M., 2002, "Effects of Local Thermal Non-Equilibrium on the Thermally Developing Forced Convection in a Porous Medium," Int. J. Heat Mass Transfer, **45**(25), pp. 4949–4955.

[3] Yang, K., and Vafai, K., 2011, "Analysis of Heat Flux Bifurcation Inside Porous Media Incorporating Inertial and Dispersion Effects-An Exact Solution," Int. J. Heat Mass Transfer, **54**(25), pp. 5286–5297.

[4] Chen, G. M., and Tso, C. P., 2012, "Field Synergy Principle Analysis on Convective Heat Transfer in Porous Medium With Uniform Heat Generation for Thermally Developing Flow," Int. J. Heat Mass Transfer, **55**(15–16), pp. 4139–4147.

[5] Ouyang, X. L., Vafai, K., and Jiang, P. X., 2013, "Analysis of Thermally Developing Flow in Porous Media Under Local Thermal Non-Equilibrium Conditions," Int. J. Heat Mass Transfer, **67**(12), pp. 768–775.

[6] Wang, K. Y., Tavakkoli, F., Wang, S. J., and Vafai, K., 2015, "Forced Convection Gaseous Slip Flow in a Porous Circular Microtube: An Exact Solution," Int. J. Therm. Sci., **97**, pp. 152–162.

[7] Wang, K. Y., Tavakkoli, F., and Vafai, K., 2015, "Analysis of Gaseous Slip Flow in a Porous Micro-Annulus Under Local Thermal Non-Equilibrium Condition—An Exact Solution," Int. J. Heat Mass Transfer, **89**(5), pp. 1331–1341.

[8] Wang, K. Y., Tavakkoli, F., Wang, S. J., and Vafai, K., 2015, "Analysis and Analytical Characterization of Bioheat Transfer During Radiofrequency Ablation," J. Biomech., **48**(6), pp. 930–940.

[9] Chen, Z. Q., Cheng, P., and Hsu, C. T., 2000, "A Theoretical and Experimental Study on Stagnant Thermal Conductivity of Bi-Dispersed Porous Media," Int. Commun. Heat Mass Transfer, **27**(5), pp. 601–610.

[10] Chen, Z. Q., Cheng, P., and Zhao, T. S., 2000, "An Experimental Study of Two Phase Flow and Boiling Heat Transfer in Bi-Dispersed Porous Channels," Int. Commun. Heat Mass Transfer, **27**(3), pp. 293–302.

[11] Nield, D. A., and Kuznetsov, A. V., 2004, "Forced Convection in a Bi-Disperse Porous Medium Channel: A Conjugate Problem," Int. J. Heat Mass Transfer, **47**(24), pp. 5375–5380.

[12] Petersen, E. E., 1991, "Adsorption in Bidisperse-Pore Systems," AICHE J., **37**(5), pp. 671–678.

[13] Semenic, T., Lin, Y. Y., Catton, I., and Sarraf, D. B., 2008, "Use of Biporous Wicks to Remove High Heat Fluxes," Appl. Therm. Eng., **28**(4), pp. 278–283.

[14] Qu, Y., Zhou, K., Zhang, K. F., and Tian, Y., 2016, "Effects of Multiple Sintering Parameters on the Thermal Performance of Bi-Porous Nickel Wicks in Loop Heat Pipes," Int. J. Heat Mass Transfer, **99**, pp. 638–646.

[15] Hooman, K., and Maas, U., 2014, "Theoretical Analysis of Coal Stockpile Self-Heating," Fire Saf. J., **67**(7), pp. 107–112.

[16] Nield, D., and Kuznetsov, A. V., 2005, "A Two-Velocity Two-Temperature Model for a Bi-Dispersed Porous Medium: Forced Convection in a Channel," Transport Porous Med., **59**(3), pp. 325–339.

[17] Nield, D. A., and Kuznetsov, A. V., 2006, "Thermally Developing Forced Convection in a Bidisperse Porous Medium," J. Porous Media, **9**(5), pp. 393–402.

[18] Kuznetsov, A. V., and Nield, D. A., 2010, "Forced Convection in a Channel Partly Occupied by a Bidisperse Porous Medium: Asymmetric Case," Int. J. Heat Mass Transfer., **53**(23), pp. 5167–5175.

[19] Kuznetsov, A. V., and Nield, D. A., 2011, "Forced Convection in a Channel Partly Occupied by a Bidisperse Porous Medium: Symmetric Case," ASME J. Heat Transfer, **133**(7), p. 072601.

[20] Narasimhan, A., and Reddy, B. V. K., 2011, "Laminar Forced Convection in a Heat Generating Bi-Disperse Porous Medium Channel," Int. J. Heat Mass Transfer, **54**(1), pp. 636–644.

[21] Narasimhan, A., Reddy, B. V. K., and Dutta, P., 2012, "Thermal Management Using the Bi-Disperse Porous Medium Approach," Int. J. Heat Mass Transfer, **55**(4), pp. 538–546.

[22] Ajay, K. P. V., Giranchandran, A. C., and Kamath, P. M., 2013, "A Numerical Investigation to Improve Heat Transfer Using Bi-Disperse Porous Heat Sink," Int. J. Technol. Eng. Sci., **1**(5), pp. 445–453.

[23] Nield, D. A., and Kuznetsov, A. V., 2006, "The Onset of Convection in a Bidisperse Porous Medium," Int. J. Heat Mass Transfer, **49**(17), pp. 3068–3074.

[24] Straughan, B., 2009, "On the Nield-Kuznetsov Theory for Convection in Bidispersive Porous Media," Transport Porous Med., **77**(2), pp. 159–168.

[25] Nield, D. A., and Kuznetsov, A. V., 2008, "Natural Convection About a Vertical Plate Embedded in a Bidisperse Porous Medium," Int. J. Heat Mass Transfer, **51**(7–8), pp. 1658–1664.

[26] Rees, D. A. S., Nield, D. A., and Kuznetsov, A. V., 2008, "Vertical Free Convective Boundary-Layer Flow in a Bidisperse Porous Medium," ASME J. Heat Transfer, **130**(9), p. 092601.

[27] Revnic, C., Grosan, T., Pop, I., and Ingham, D. B., 2009, "Free Convection in a Square Cavity Filled With a Bidisperse Porous Medium," Int. J. Therm. Sci., **48**(10), pp. 1876–1883.

[28] Narasimhan, A., and Reddy, B. V. K., 2010, "Natural Convection Inside a Bidisperse Porous Medium Enclosure," ASME J. Heat Transfer, **132**(1), p. 012502.

[29] Narasimhan, A., and Reddy, B. V. K., 2011, "Resonance of Natural Convection Inside a Bidisperse Porous Medium Enclosure," ASME J. Heat Transfer, **133**(4), p. 042601.

[30] Cekmer, O., Mobedi, M., Ozerdem, B., and Pop, I., 2012, "Fully Developed Forced Convection in a Parallel Plate Channel With a Centered Porous Layer," Transport Porous Med., **93**(93), pp. 179–201.

[31] Mahmoudi, Y., Karimi, N., and Mazaheri, K., 2014, "Analytical Investigation of Heat Transfer Enhancement in a Channel Partially Filled With a Porous Material Under Local Thermal Non-Equilibrium Condition: Effects of Different Thermal Boundary Conditions at the Porous-Fluid Interface," Int. J. Heat Mass Transfer, **70**, pp. 875–891.

[32] Wang, B., Hong, Y., Hou, X., Xu, Z., Wang, P., Fang, X., and Ruan, X., 2015, "Numerical Configuration Design and Investigation of Heat Transfer Enhancement in Pipes Filled With Gradient Porous Materials," Energy Convers. Manage., **105**, pp. 206–215.

[33] Wang, K. Y., Vafai, K., and Wang, D. Z., 2016, "Analytical Characterization of Gaseous Slip Flow and Heat Transport Through a Parallel-Plate Microchannel With a Centered Porous Substrate," Int. J. Numer. Method Heat Fluid Flow, **26**(3/4), pp. 854–878.

[34] Dehghan, M., Valipour, M. S., and Saedodin, S., 2016, "Microchannels Enhanced by Porous Materials: Heat Transfer Enhancement or Pressure Drop Increment?" Energy Convers. Manage., **110**, pp. 22–32.

[35] Magyari, E., 2013, "Normal Mode Analysis of the High Speed Channel Flow in a Bidisperse Porous Medium," Transport Porous Med., **97**(3), pp. 345–352.

[36] Nield, D. A., and Kuznetsov, A. V., 2013, "A Note on Modeling High Speed Flow in a Bidisperse Porous Medium," Transport Porous Med., **96**(3), pp. 495–499.

[37] Cheng, C. Y., 2013, "Natural Convection Heat Transfer From an Inclined Wavy Plate in a Bidisperse Porous Medium," Int. Commun. Heat Mass Transfer, **43**, pp. 69–74.

[38] Amiri, A., Vafai, K., and Kuzay, T. M., 1995, "Effects of Boundary Conditions on Non-Darcian Heat Transfer Through Porous Media and Experimental Comparisons," Numer. Heat Transfer Appl., **27**(6), pp. 651–664.

[39] Wang, K. Y., Wang, D. Z., and Li, P. C., 2015, "Two Decoupling Methods for the Heat Transfer Model of a Plate Channel Filled With a Porous Medium," Appl. Math. Mech., **36**(5), pp. 494–504 (in Chinese).

[40] Dukhan, N., Al-Rammahi, M. A., and Suleiman, A. S., 2013, "Fluid Temperature Measurements Inside Metal Foam and Comparison to Brinkman-Darcy Flow Convection Analysis," Int. J. Heat Mass Transfer, **67**(4), pp. 877–884.